

Materials Acceleration Platform for Electrochemistry (MAP-E): a Platform for Autonomous Electrochemistry

Daniel Persaud^{1,2}, Mike Werezak¹, Mark Xu¹, Melyne Zhou², Frank Benkel¹, Xin Pang¹, Vahid Attari¹, Brian DeCost³, Ashley Dale², Nicholas Senior¹, Gabriel Birsan^{1,*}, and Jason Hatrick-Simpers^{1, 2, 4, 5, 6, **}

¹CanmetMATERIALS, Natural Resources Canada, 183 Longwood Road South, Hamilton, ON, Canada

²Department of Materials Science and Engineering, University of Toronto, 27 King's College Cir, Toronto, ON, Canada

³Material Measurement Laboratory, National Institute of Standards and Technology, 100 Bureau Dr, Gaithersburg, MD, USA

⁴Acceleration Consortium, University of Toronto, 27 King's College Cir, Toronto, ON, Canada.

⁵Vector Institute for Artificial Intelligence, 661 University Ave, Toronto, ON, Canada.

⁶Schwartz Reisman Institute for Technology and Society, 101 College St, Toronto, ON, Canada.

*Correspondence: gabriel.birsan@NRCan-RNCan.gc.ca

**Correspondence: jason.hatrick.simpers@utoronto.ca

Abstract

Corrosion testing is slow, labor-intensive, and sensitive to operator technique, limiting the generation of large, high-quality datasets for data-driven materials discovery. We introduce the Materials Acceleration Platform for Electrochemistry (MAP-E), an autonomous, high-throughput system capable of performing parallel electrochemical experiments. MAP-E integrates robotic liquid handling, sample transfer, and multi-channel potentiostatic control and extract corrosion metrics without human intervention. Validation against an ASTM G61-analog benchmark demonstrates reproducibility, with a standard deviation of 76 mV in pitting potential across 32 automated measurements. The platform was then employed to autonomously construct pH-chloride stability diagrams for 304 stainless steel using an uncertainty-driven sampling strategy on a Gaussian Process surrogate model. This approach reduces operator involvement and accelerates the exploration of environmental spaces. MAP-E establishes a framework for autonomous electrochemical experimentation, enabling generation of corrosion datasets that inform materials discovery, alloy design, and durability assessment in service environments.

1 Introduction

The corrosion of metals and alloys remains a major challenge in ensuring the safety and reliability of infrastructure, transportation, and energy systems [1–3]. During service, materials are exposed to a diverse range of complex environments that can accelerate degradation, leading to significant safety concerns and as a results, substantial economic cost [2–8]. Predicting how materials will perform under different service conditions, or designing new materials with improved corrosion resistance for specific environments, requires an understanding of the complex interplay between alloy chemistry, microstructure, surface condition, and environmental factors [9–11]. This multifaceted nature makes the systematic exploration of corrosion phenomena experimentally demanding, especially because traditional electrochemical experiments are labor-intensive and sensitive to procedural details, requiring considerable experience to achieve reproducible results [3,12]. As a result, generating large, high-quality datasets that capture corrosion behavior across broad parameter spaces is challenging, limiting the ability to establish predictive relationships between material properties, environment, and degradation mechanisms.

Autonomous electrochemical platforms have the potential to address these challenges by integrating networked instrumentation, modular fluid handling, and parallelized electrochemical cells under unified control software [8,13,14]. When coupled with machine learning (ML), these systems can be used to generate high-quality, informative data that enable systematic exploration of complex experimental spaces and discovery of underlying patterns. The standardized data produced can be shared with the broader research community, enabling others to develop predictive models, identify promising research directions, and collaborate to accelerate innovation across the field.

Recent years have seen substantial progress in high-throughput (HT) electrochemical platforms, including systems that integrate hardware and software to enable varying degrees of autonomous operation. Early HT approaches emphasized parallel screening to maximize throughput, often relying on shared electrolytes, reduced solution volumes, simplified electrode configurations, or measurements limited to post-exposure or optical characterization [15–19]. More recent efforts have shifted toward increased autonomy through integrated hardware–software platforms, commonly based on scanning droplet cells or gantry-based systems that sequentially position a shared reference and counter electrode into electrolyte-filled wells [20–29]. Despite these advances, most

platforms face trade-offs: systems closer to autonomy often perform experiments serially, limiting exploration speed, whereas parallelized systems frequently compromise on experimental fidelity, restricting their relevance for corrosion science. These accommodations are typically driven by constraints in hardware, cost, or the complexity associated with linking multiple pieces of equipment [30,31]. Collectively, these limitations define a critical gap for corrosion research: the absence of a platform that can perform parallel electrochemical measurements, using traditional cell geometries, electrolyte volumes, and standard electrode configurations, features necessary for high-quality data-driven exploration across diverse material-environment combinations.

To address this gap, we have developed the Materials Acceleration Platform for Electrochemistry (MAP-E), a flexible, HT platform designed for autonomous electrochemical experiments. It integrates eight individually addressable electrochemical cells, each capable of performing independent measurements in parallel. The platform features modular fluid handling, enabling exploration of a wide range of aqueous environments. Robust component control and scheduling software manages complex experimental campaigns, enabling autonomous operation.

By generating standardized electrochemical data, the MAP-E serves as a foundation for applying ML algorithms to autonomously explore complex experimental spaces. In this work, we first validate the MAP-E’s ability to perform reproducible electrochemical measurements using a modified testing protocol derived from an established corrosion standard. We then demonstrate its capacity to autonomously construct information-rich stability diagrams within a single closed-loop campaign, enabling more efficient use of experimental resources and operator time than traditional sequential approaches. By running eight cells in parallel, MAP-E achieves an immediate eightfold increase in throughput. Once the initial stock solutions are prepared, the system mixes and explores a broad environmental grid without further human intervention, enabling unattended execution of experimental campaigns. An uncertainty-driven acquisition strategy is used to adaptively select subsequent experimental conditions based on the model’s posterior predictive uncertainty. This focuses sampling on regions where the model is least certain, allowing informative areas of the design space to be explored efficiently under a constrained experimental budget. With these capabilities, MAP-E provides a framework for reproducible, data-driven exploration of corrosion phenomena and supports scalable generation of high-quality electrochemical datasets, enabling broader collaboration and innovation across the electrochemistry community.

2 Methods

The design philosophy of the MAP-E centers on maximizing experimental throughput while minimizing the trade-offs in versatility and flexibility that commonly constrain automated or autonomous electrochemical platforms. Prior to operation, stock solutions are prepared to span the target environmental range, and polished samples are loaded into dedicated sample racks. A high-level software interface accepts experiment requests which specify the electrochemical methods, sample selection, and environmental conditions. Once initiated, MAP-E automatically orchestrates the full workflow. The system loads samples into the electrochemical cells, mixes and dispenses the target electrolyte compositions via the liquid-handling system. It executes the prescribed electrochemical measurements, and processes the resulting data to extract the corrosion parameters of interest while the system cleans the cells and prepares for the next round of experiments. The following sections describe the hardware, control software, and modeling framework for the autonomous stability diagram investigation.

2.1 Hardware

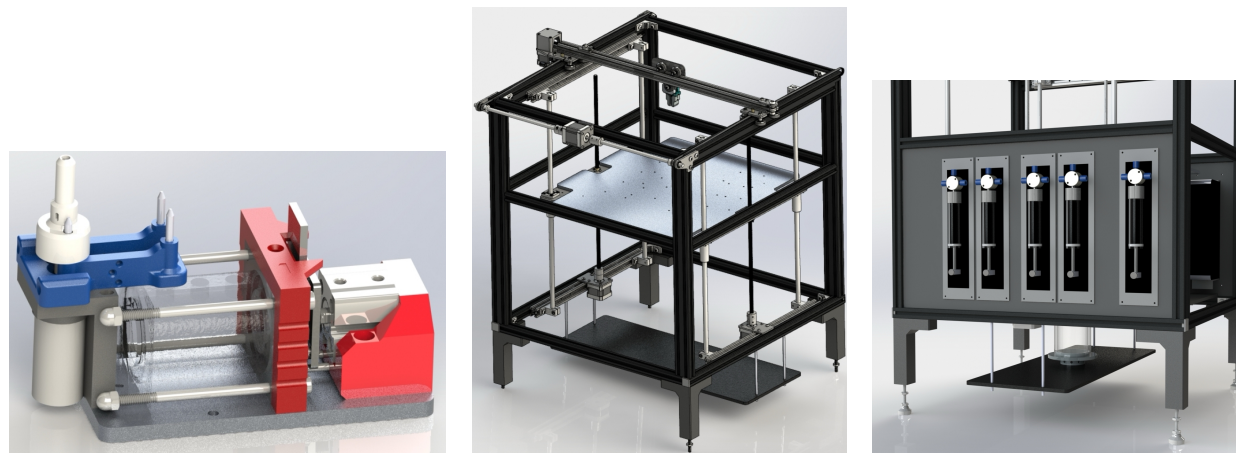
The MAP-E hardware is organized into four subsystems that enable automated, HT electrochemical experiments: (1) the electrochemical cell array, (2) gantry system, (3) liquid handling, and (4) the potentiostat. The electrochemical array consists of eight custom, independently addressable flat cells, constructed from a cylindrical polycarbonate body with two machined end caps (one cell is shown in Figure 1a). Each cell incorporates a platinum mesh counter electrode mounted within the rear end cap housing and a 1 cm^2 exposure window sealed with a Viton o-ring in the front end cap, defining a 25 mL electrolyte volume that meets the 0.2 mL/mm^2 minimum ratio recommended by ASTM G31 [32].

A pneumatic cylinder mounted on the front end cap secures the sample against the o-ring to ensure a consistent, leak-free seal. Samples are transferred from one of two sample racks, each accommodating 16 samples ($60 \text{ mm} \times 20 \text{ mm} \times 3 \text{ mm}$) to the cells using a Cartesian gantry system built from a retrofitted 3D printer. This serves as the structural backbone of the platform, supporting the dosing pumps, mixing tank, electronics, and electrochemical cell array (Figure 1b). The gantry system is also used to transfer the CH Instruments Ag/AgCl reference electrodes from

their storage locations (1 mol/L KCl) into the cells.

Liquid handling is performed by a network of ten 25 mL Tricontinent CX6000 dosing pumps with multi-port valves, all connected to a central mixing tank that houses a pH meter and magnetic stir bar (Figure 1c). Eight of the pumps are dedicated to electrolyte delivery from the mixing tank and removal to waste for each of the cells, while the remaining two are used to fill the mixing tank with stock and cleaning solutions.

A Bio-Logic VMP-3 multichannel potentiostat provides independent control of the eight cells. Electrical connections are routed through a custom-designed breakout box with gold-plated connectors, ensuring reliable contact and straightforward configuration. Together, these subsystems enable parallel, flexible electrochemical experimentation across conditions while maintaining the form factor, electrolyte volumes, and experimental fidelity of traditional cells.



(a) Custom electrochemical flat cell with pneumatic clamping mechanism and integrated electrodes (reference electrode in storage tube on the left.)

(b) Gantry system adapted from a 3D printer, supporting sample transfer and component mounting.

(c) Liquid handling system with dosing pumps and central mixing tank attached to the gantry frame.

Figure 1: Key hardware subsystems of the MAP-E platform.

2.2 Control Software

The MAP-E control software was developed as a modular framework for automated, concurrent experimentation. The architecture comprises three layers: (1) the application server, (2) the experiment execution engine, and (3) the instrument driver libraries, shown in Figure 2. Together, these layers abstract the underlying hardware complexity and provide a high-level user interface for submitting experiment requests.

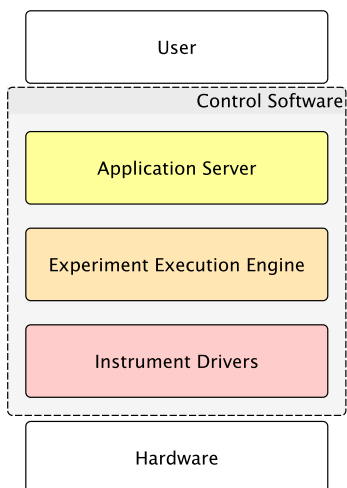


Figure 2: Schematic of the MAP-E software architecture, illustrating the three primary layers: application server, experiment execution engine, and instrument driver libraries.

The application server provides a network-accessible interface for managing experiment requests and coordinating the flow of data. The server accepts experiment specifications as structured inputs, handles data collection and storage automatically, and maintains a registry of active and completed jobs to support asynchronous submission, execution, and monitoring. At the core of the control architecture is the experiment execution engine, which orchestrates real-time operation of the hardware subsystems shown in Figure 1. Experimental procedures are defined as sequences of schedulable tasks (e.g., sample transfer, cell filling, electrochemi-

cal techniques) that are dynamically allocated to available cells or shared resources (e.g., the mixing tank), as illustrated in Figure 3. This architecture supports fully concurrent operation, allowing multiple experiments to proceed in parallel, while managing shared hardware dependencies transparently. The instrument driver libraries form the interface layer between the execution engine and the physical devices. Each driver exposes the essential functions of its corresponding hardware—such as pumps, actuators, or potentiostat channels—through a consistent software interface, enabling coordination within the broader system. Its modular design allows new instruments or sensors to be incorporated with minimal software modification. Collectively, these components enable a straightforward transition toward adaptive or data-driven experimental campaigns.

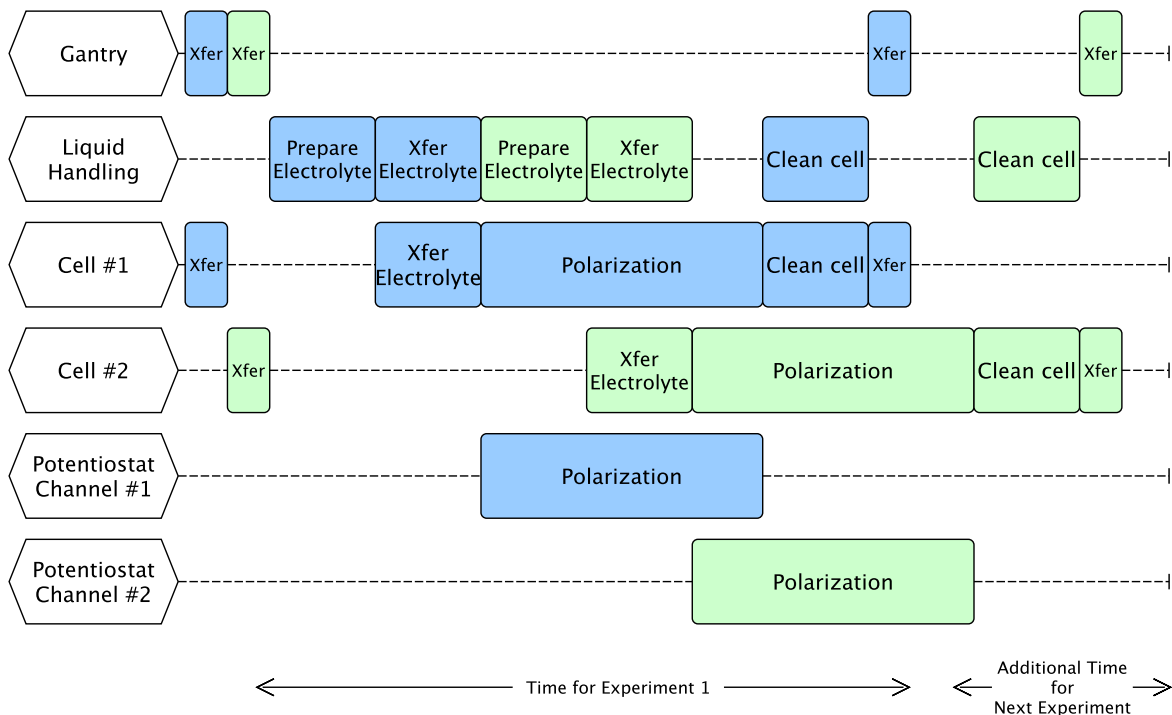


Figure 3: Illustration of the resource allocation and scheduling framework within the experiment execution engine, demonstrating parallel operation of multiple electrochemical cells while managing shared resources like the mixing tank. In this example, separate experiments are denoted by different colors and only two cells are shown for clarity.

2.3 Adaptive Experimentation Framework

In this work, we perform potentiodynamic polarization (PP) measurements across a predefined grid of pH values (3 to 10) and chloride ion concentrations (0 mol/L to 0.1 mol/L) to construct empirical stability diagrams. The rationale for this approach will be discussed in section 3. Following each experiment, the resulting data is retrieved from the control software to a user-specified directory. Data is processed automatically, and new experiment requests can then be generated and submitted back to the control software.

The raw PP data is analyzed using a Python-based pipeline that identifies the corrosion potential (E_{corr}) and pitting potential (E_{pit}). The current response is first smoothed using a Savitzky–Golay filter, and the derivative of current density with respect to potential is computed to locate maxima corresponding to the onset of stable pitting. The E_{corr} is the potential at the minimum absolute current, and E_{pit} is identified as the first major derivative peak occurring above

$E_{\text{corr}} + 0.1 \text{ V}$ (Supplemental Figure S1). These parameters are stored and made available for subsequent modeling.

A Gaussian Process (GP) regression model serves as the surrogate model for predicting E_{pit} across the design space. The GP employs a scaled Matérn covariance kernel ($\nu = 2.5$) with automatic relevance determination (ARD) to capture varying correlation length scales in each input dimension. A heteroscedastic likelihood is used to represent measurement-dependent noise, accounting for variability between duplicate experiments. The model is initialized with four Latin hypercube-sampled (LHS) conditions and iteratively updated as new data are collected. Experimental selection is guided by an uncertainty-driven acquisition function that prioritizes conditions with the highest posterior predictive variance in E_{pit} . This approach directs the MAP-E toward regions of high model uncertainty or experimental disagreement, balancing exploration of untested conditions with refinement of noisy regions. Together, the automated data extraction, surrogate modeling, and adaptive selection modules form a closed-loop, adaptive framework for data-efficient mapping of corrosion behavior. With the adaptive experimental framework established, we first demonstrate the MAP-E’s capability to generate reliable corrosion data, and then apply it to construct stability diagrams across a range of environmental conditions.

2.4 Materials and Sample Preparation

Standard Type 304 stainless steel (UNS S30400) sheet stock was procured from McMaster-Carr, water-jet cut to size, and polished to 600-grit following ASTM G61. For the validation study, a 3.56 wt% sodium chloride solution was prepared according to ASTM G61 [33]. For the autonomous stability diagram experiments, stock solutions for the Britton-Robinson (BR) [34] buffer were prepared using reagent-grade chemicals at the following concentrations: sodium hydroxide (0.3 mol/L), phosphoric acid (0.2 mol/L), acetic acid (0.2 mol/L), and boric acid (0.2 mol/L). Two sodium chloride stock solutions were also prepared to span the chloride range: 0.04 mol/L and 0.4 mol/L. All solutions were made with type 1 water (resistivity $>18 \text{ mol/L}\cdot\Omega\cdot\text{cm}^2$ at 25 °C) and used to generate the desired electrolyte compositions for their respective experiments.

3 Results and Discussion

3.1 Corrosion Validation

As discussed above, the design and configuration of automated or autonomous electrochemical platforms vary widely, making comparison across laboratories difficult [14]. Even with eight independent cells, intra-platform reproducibility must be verified [35]. Accordingly, we aim to validate the electrochemical performance of the MAP-E using experiments aligned with standards commonly employed in corrosion testing to assess cell-to-cell reproducibility. These experiments are performed to demonstrate that the MAP-E can generate reliable electrochemical data suitable for subsequent adaptive experimentation.

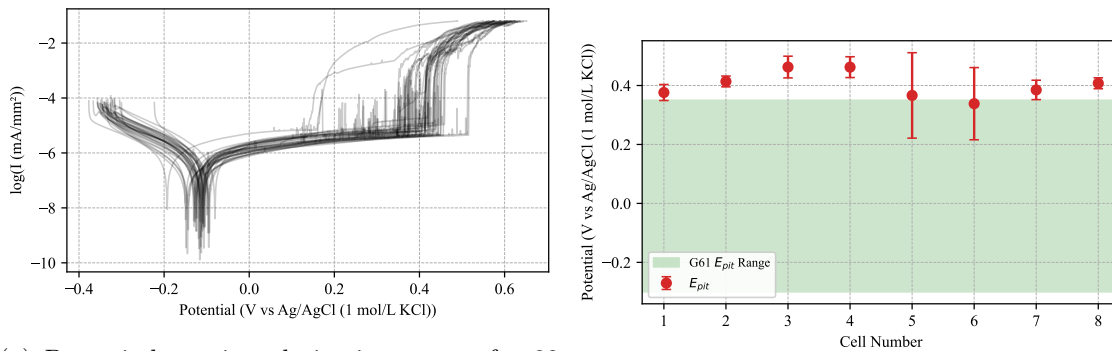
To validate the electrochemical performance of the MAP-E we performed PP experiments using an analog to ASTM G61 [33], a standard for evaluating localized corrosion susceptibility of alloys in aqueous chloride environments. Following as closely as possible the procedure’s allows us to quantitatively benchmark the MAP-E’s performance against established inter-laboratory reproducibility metrics for E_{pit} . Adhering closely to a standard procedure enables quantitative benchmarking of the MAP-E’s performance against established inter-laboratory reproducibility metrics for E_{pit} .

Several adaptations to ASTM G61 were made to accommodate the MAP-E architecture. The platform operates under ambient (aerated) conditions rather than the nitrogen-deaerated environment specified by ASTM G61. An Ag/AgCl (1 mol/L KCl) reference electrode was used in place of the saturated calomel electrode primarily due to its compatibility with MAP-E’s automated handling system, lower maintenance requirements, and reduced toxicity, while still providing stable performance in chloride-containing electrolytes. Additionally, the specimen holder was implemented using the MAP-E’s custom flat-cell design, and tests were performed at room temperature, as opposed to the 25 °C specified in the standard. While these modifications reflect practical aspects of operating an autonomous, multi-cell platform, the essential elements of the ASTM G61 methodology; electrolyte composition, electrochemical parameters, and interpretation of E_{pit} , were preserved, enabling a direct and meaningful assessment of MAP-E’s electrochemical capability.

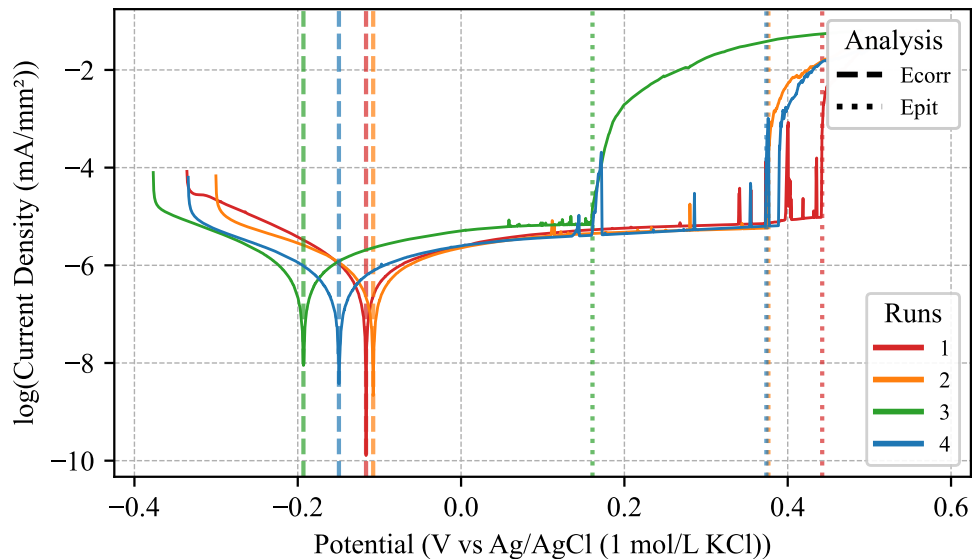
ASTM G61 defines expected inter-laboratory reproducibility and bias in E_{pit} during PP measurements. Based on results from five independent laboratories, the standard reports an inter-

laboratory 2σ of ≈ 600 mV in E_{pit} . However, it does not define intra-laboratory repeatability, leaving the expected variability when multiple identical tests are performed within a single laboratory, or in the case of the MAP-E, a single cell, unspecified.

Figure 4 shows the results from the ASTM G61-analog validation experiments. Thirty-two 304 stainless steel samples were polished per the ASTM procedure and tested across four full MAP-E runs (eight cells per run). After a 1 hour rest, PP was performed in aerated aqueous NaCl solution with mass fraction of 3.56 wt. % at room temperature at a scan rate of 0.167 mV s $^{-1}$, sweeping from -250 mV vs. E_{corr} until a cell current of 5 mA was reached.



(a) Potentiodynamic polarization curves for 32 type 304 stainless steel samples in aerated aqueous NaCl solution with mass fraction of 3.56 wt. % at room temperature, measured across the eight cells of the MAP-E. (b) Distribution of E_{pit} extracted from the polarization curves, showing cell-to-cell variability and overall reproducibility. Error bars indicate spread across measurements within each cell.



(c) Polarization curves from just one cell (Cell 6) to illustrate run-to-run variability within a single cell.

Figure 4: Results from the ASTM G61 replication experiments with the MAP-E.

Across the 32 measurements, the mean E_{corr} was $-119 \text{ mV} \pm 21 \text{ mV}$ and the mean E_{pit} was $402 \text{ mV} \pm 76 \text{ mV}$ (Figure 4a). The standard deviation of E_{pit} across MAP-E measurements is approximately four times smaller than the inter-laboratory standard deviation implied by ASTM G61 ($\approx 300 \text{ mV}$, based on a reported two-standard-deviation spread of $\approx 600 \text{ mV}$ across multiple laboratories). At the cell level, variability was even tighter, with standard deviations typically $< 40 \text{ mV}$ (Figure 4b), demonstrating consistent performance in repeated tests within individual cells—an analogue to intra-laboratory repeatability, which ASTM G61 does not define. The E_{pit} values obtained on the MAP-E were consistently higher than those reported in ASTM G61 datasets, with individual measurements up to $\approx 120 \text{ mV}$ higher and a mean positive offset of $\approx 50 \text{ mV}$.

The MAP-E results demonstrate high reproducibility and precision, with intra-cell and inter-cell variability well below the inter-laboratory spread defined in ASTM G61. The elevated average E_{pit} and the measurement noise in the passive region are both attributable to testing in aerated electrolyte. Dissolved oxygen increases cathodic reaction kinetics and promotes passive film stabilization, which shifts the pitting potential positively relative to deaerated ASTM conditions [36]. The oxygen also introduces metastable pitting events that manifest as small fluctuations in the current response near E_{pit} [37]. This behavior is illustrated in Figure 4c, where two nominally identical runs (3 & 4) produced early pit initiation during the passive region: in one run the metastable pit transitioned into stable pit growth, while in the other it repassivated at approximately the same potential. Notably, these “early-pit” events occur near the mean E_{pit} reported in ASTM G61, further supporting that the observed differences arise from environmental aeration.

In addition to producing measurement quality consistent with established corrosion test standards, the MAP-E executes all steps of the experiment automatically once samples and stock solutions are setup. In this validation study, eight cells are operated in parallel, enabling all the potentiodynamic tests to be completed with minimal operator involvement beyond routine monitoring over the course of two days. Although the electrochemical runtime remains comparable to conventional testing, operator time is reduced substantially. This capability positions the MAP-E to not only accelerate data generation, but also to support quantitative, data-drive studies.

3.2 Building Information-Rich Stability Diagrams Autonomously

Having established the MAP-E’s reproducibility and precision, we deployed the platform to autonomously generate empirical corrosion stability diagrams. Traditional stability diagrams, such as Pourbaix diagrams, describe the thermodynamic stability of metals [38], while experimentally generated diagrams relating applied potential to pitting susceptibility, such as Pedefferri diagrams [39, 40], are typically constructed manually and limited to a small number of discrete conditions. The MAP-E extends this approach by performing PP experiments across pH-chloride space and selecting subsequent conditions based on model-predicted uncertainty. A GP surrogate model predicts the E_{pit} throughout the design space, and an uncertainty-driven acquisition function guides the platform toward the most informative regions, reducing redundant experiments, as described in section 2.3. While demonstrated here for 304 stainless steel, this workflow is generalizable, enabling efficient, autonomous mapping of corrosion susceptibility and understanding of the service envelope of materials across complex environmental conditions.

The exploration space for autonomous corrosion mapping was defined in terms of pH and chloride ion concentration, two critical variables controlling corrosion behavior for stainless steels and following the concept of Pedefferri diagrams [39, 40]. The MAP-E investigated environments spanning pH 3 to 10.5 (0.5-unit increments) and chloride concentrations from 0 mol/L to 0.1 mol/L (semi-logarithmic increments), encompassing 80 unique conditions. Each environment was formulated using a BR buffer as the background electrolyte to maintain pH stability while covering a broad range of pH values from a limited set of stock solutions, with controlled additions of sodium chloride stocks achieving the target chloride concentrations. A Python-based framework calculates the precise stock volumes to reach the target pH and chloride concentration, after which the liquid handling system automatically prepares each condition and measures the pH in the mixing tank. We observed that the measured pH differ slightly from the target value due to the pumping accuracy but the pH is always measured in the mixing tank prior to dispensing and the measured value that is used for subsequent modeling. Each condition was then characterized electrochemically using the same PP parameters as in the section 3.1, with the automated data extraction workflow described in section 2.3, generating the corrosion parameters E_{pit} for the subsequent modeling.

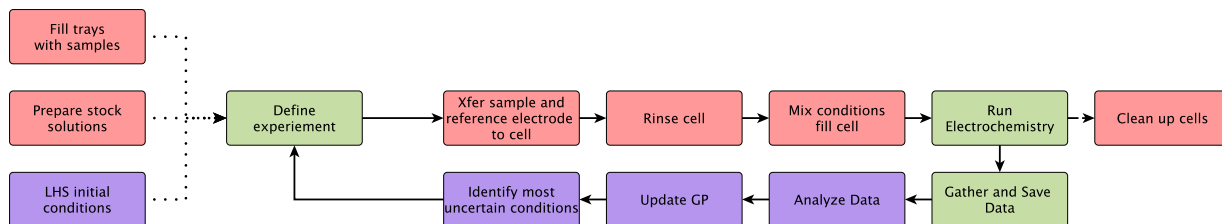
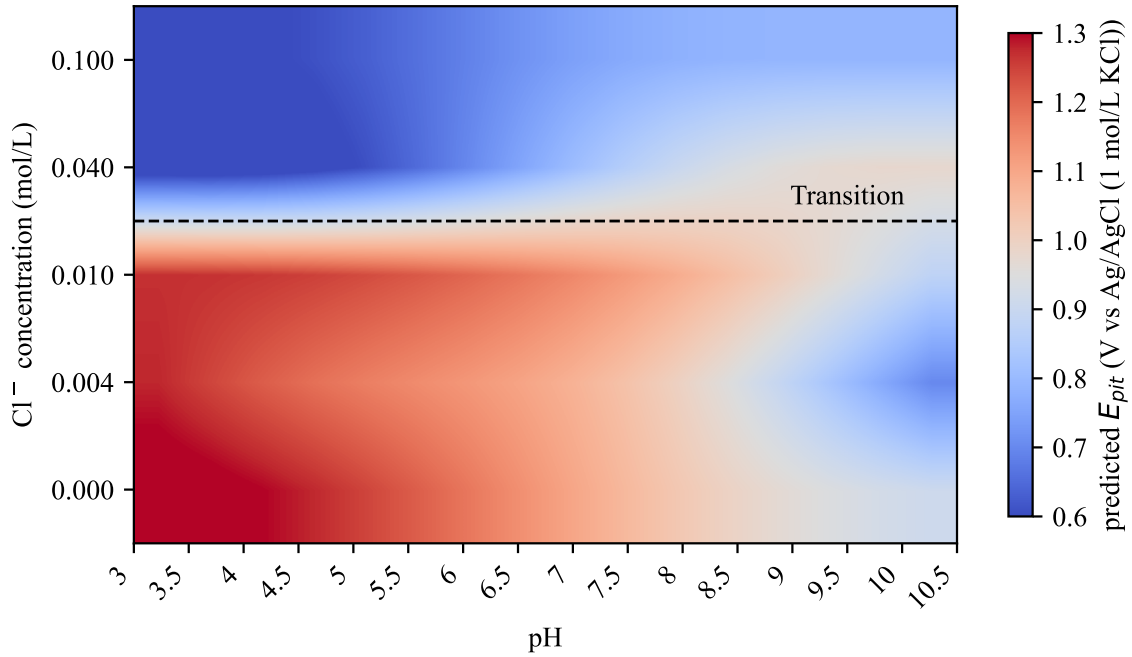
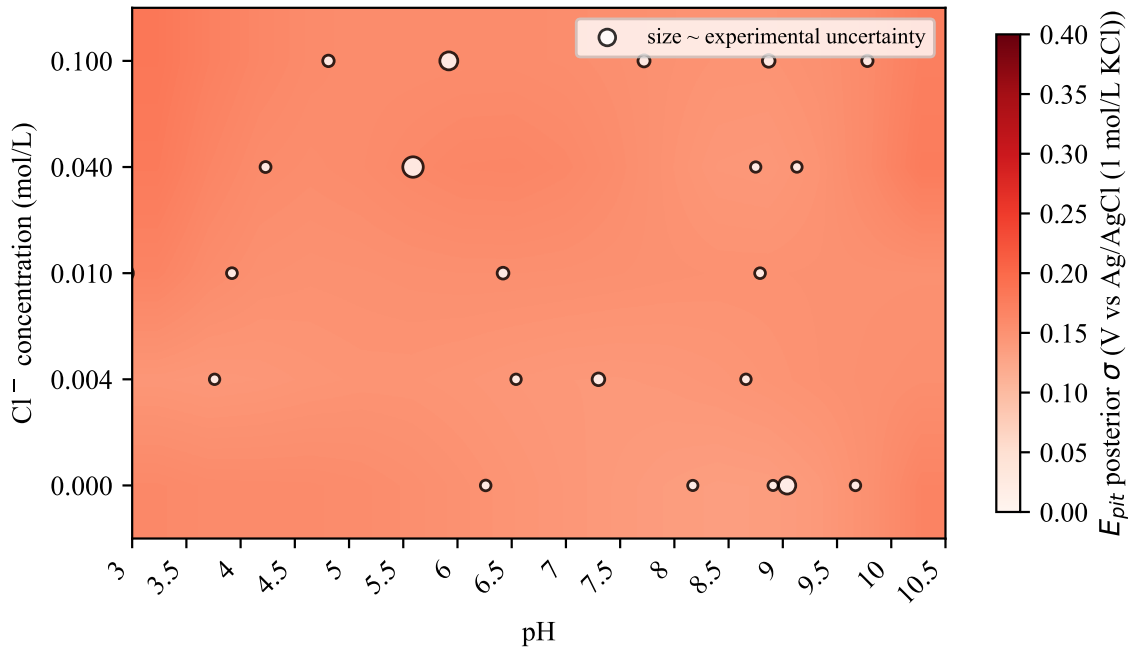


Figure 5: High-level workflow diagram of the autonomous experimental workflow for constructing pH-Cl⁻ stability diagrams using the MAP-E platform. The red boxes indicate steps that can primarily be associated with the hardware, the green boxes indicate software-driven steps, and the purple boxes indicate the adaptive modeling components.

The autonomous experimental workflow is illustrated in Figure 5. The campaign was initialized with four conditions selected using Latin hypercube sampling (LHS), with duplicate measurements for each condition to capture intrinsic variability and model experimental noise. After the initial measurements, the MAP-E proceeded with a fixed budget of 48 additional samples (three trays, 24 conditions in duplicate), autonomously selecting subsequent conditions according to the uncertainty-driven sampling strategy described in section 2.3. These steps provide a systematic method of exploring environmental space to construct empirical stability diagrams (Figure 6).



(a) Stability diagram showing the predicted E_{pit} across the pH- Cl^- space for 304 stainless steel, generated autonomously by the MAP-E.



(b) Uncertainty map corresponding to the stability diagram, highlighting regions where the model is less certain about E_{pit} predictions.

Figure 6: Autonomously generated stability diagrams for 304 stainless steel in pH- Cl^- space, illustrating the predicted E_{pit} and associated uncertainty in the form of posterior predictive standard deviation.

The resulting stability diagram (Figure 6a) shows that 304 stainless steel is least susceptible to pitting in oxygenated, moderately acidic, low-chloride environments and most susceptible under high-chloride, acidic conditions. In general, increasing chloride concentration leads to decreasing pitting potentials, indicating greater susceptibility to localized corrosion. A transition region appears between 0.01 mol/L and 0.04 mol/L chloride, centered near 0.025 mol/L, above which E_{pit} decreases with decreasing pH, while below this threshold a different pH dependence is observed.

The GP-derived stability diagram resolves this change in behavior across the pH–chloride space without imposing any mechanistic assumptions. At high chloride concentrations, the observed trends are consistent with established understanding: sufficient chloride promotes pit initiation, while decreasing pH further destabilizes the passive film and lowers the potential required for pit propagation [41, 42]. Under these conditions, the combined effects of aggressive anion adsorption and reduced oxide stability dominate the pitting response.

In contrast, below the transition region, chloride concentrations are insufficient to strongly control pit initiation, and the observed variation in E_{pit} with pH reflects predominantly electrochemical effects rather than chloride-driven pitting chemistry. In this low-chloride regime, the GP predicts an approximately linear decrease in E_{pit} with increasing pH, with a slope of 62 mV per pH unit (Supplementary Figure S2), closely matching the Nernstian shift (-59 mV per pH unit at 25 °C) [43] expected for electrode potentials referenced to Ag/AgCl under ambient aeration. This agreement emerges purely from the experimental data and indicates that, in the absence of sufficient chloride, the measured pitting potential is governed largely by the underlying electrochemical potential scale rather than by localized corrosion processes.

The posterior predictive uncertainty map (Figure 6b) highlights regions where additional data would most improve model confidence, with higher uncertainty near the boundaries of the design space where experimental coverage is sparse. Despite these localized regions, the uncertainty surface remains relatively uniform, with an average predictive uncertainty of ≈ 150 mV. Together, these results define the service envelope of 304 stainless steel across the investigated pH–chloride space and demonstrate that the MAP-E platform can autonomously generate information-rich stability diagrams suitable for guiding future experimentation.

4 Conclusions

We present the Materials Acceleration Platform for Electrochemistry (MAP-E), a modular, HT system capable of autonomously performing parallel electrochemical experiments with individually addressable cells. Validation against a ASTM G61-analog benchmark confirms reproducibility and quantitative precision, with standard deviations in E_{pit} approximately one quarter of the inter-laboratory variability reported in the standard, producing data suitable for rigorous analysis. Using a posterior-uncertainty-driven experimental framework, MAP-E autonomously generated empirical pH-chloride stability diagrams for 304 stainless steel, efficiently capturing key trends in pitting susceptibility and associated uncertainties. The platform’s architecture enables closed-loop experimentation: selecting, executing, and analyzing experiments without human intervention, while supporting flexible definition of electrochemical workflows beyond corrosion testing. Collectively, these results establish MAP-E as a generalizable and data-efficient framework for mapping corrosion service envelopes, and demonstrate its potential to accelerate both corrosion research and broader electrochemical discovery efforts.

References

- [1] J. Cabana, T. Alaan, G. W. Crabtree, M. C. Hatzell, K. Manthiram, D. A. Steingart, I. Zenyuk, F. Jiao, A. Vojvodic, J. Y. Yang, N. P. Balsara, K. A. Persson, D. J. Siegel, C. L. Haynes, J. Mauzeroll, M. Shen, B. J. Venton, N. Balke, J. Rodríguez-López, D. R. Rolison, R. Shahbazian-Yassar, V. Srinivasan, S. Chaudhuri, A. Couet, and J. Hatrick-Simpers, “NGenE 2021: Electrochemistry Is Everywhere,” *ACS Energy Lett.*, vol. 7, no. 1, pp. 368–374, Jan. 2022.
- [2] M. Iannuzzi and G. S. Frankel, “The carbon footprint of steel corrosion,” *npj Mater Degrad*, vol. 6, no. 1, p. 101, Dec. 2022.
- [3] D.-H. Xia, C.-M. Deng, D. Macdonald, S. Jamali, D. Mills, J.-L. Luo, M. G. Strebl, M. Amiri, W. Jin, S. Song, and W. Hu, “Electrochemical measurements used for assessment of corrosion and protection of metallic materials in the field: A critical review,” *Journal of Materials Science & Technology*, vol. 112, pp. 151–183, Jun. 2022.
- [4] A. Groysman, *Corrosion Monitoring*. Dordrecht: Springer Netherlands, 2010, pp. 189–230.
- [5] G. Koch, J. Varney, N. Thompson, O. Moghissi, M. Gould, and J. Payer, “International measures of prevention, application, and economics of corrosion technologies study,” *NACE int*, vol. 216, no. 3, 2016.
- [6] G. Koch, “Cost of corrosion,” in *Trends in Oil and Gas Corrosion Research and Technologies*. Elsevier, 2017, pp. 3–30.
- [7] R. Bender, D. Féron, D. Mills, S. Ritter, R. Bäßler, D. Bettge, I. De Graeve, A. Dugstad, S. Grassini, T. Hack, M. Halama, E.-H. Han, T. Harder, G. Hinds, J. Kittel, R. Krieg, C. Leygraf, L. Martinelli, A. Mol, D. Neff, J.-O. Nilsson, I. Odnevall, S. Paterson, S. Paul, T. Prošek, M. Raupach, R. I. Revilla, F. Ropital, H. Schweigart, E. Szala, H. Terryn, J. Tidblad, S. Virtanen, P. Volovitch, D. Watkinson, M. Wilms, G. Winning, and M. Zheludkevich, “Corrosion challenges towards a sustainable society,” *Materials & Corrosion*, vol. 73, no. 11, pp. 1730–1751, Nov. 2022.

- [8] M. A. Pence, G. Hazen, and J. Rodríguez-López, “The emergence of automation in electrochemistry,” *Current Opinion in Electrochemistry*, vol. 51, p. 101679, Jun. 2025.
- [9] M. Nnoka, T. Alaso Jack, and J. Szpunar, “Effects of different microstructural parameters on the corrosion and cracking resistance of pipeline steels: A review,” *Engineering Failure Analysis*, vol. 159, p. 108065, May 2024.
- [10] K. Hariharan and S. Virtanen, “Microstructure engineering for corrosion resistance in structural alloy design,” *npj Mater Degrad*, vol. 8, no. 1, p. 115, Nov. 2024.
- [11] W. Chen, L. Ma, Y. Li, D. Wu, K. Zhou, J. Wang, Z. Chen, X. Guo, Z. Li, T. Chowwanonthapunya, X. Li, and D. Zhang, “Prediction of coating degradation based on “Environmental Factors–Physical Property–Corrosion Failure” two-stage machine learning,” *npj Mater Degrad*, vol. 9, no. 1, p. 67, Jun. 2025.
- [12] A. Hussein Khalaf, Y. Xiao, N. Xu, B. Wu, H. Li, B. Lin, Z. Nie, and J. Tang, “Emerging AI technologies for corrosion monitoring in oil and gas industry: A comprehensive review,” *Engineering Failure Analysis*, vol. 155, p. 107735, Jan. 2024.
- [13] S. P. Stier, C. Kreisbeck, H. Ihssen, M. A. Popp, J. Hauch, K. Malek, M. Reynaud, T. Goumans, J. Carlsson, I. Todorov, L. Gold, A. Räder, W. Wenzel, S. T. Bandesha, P. Jacques, F. Garcia-Moreno, O. Arcelus, P. Friederich, S. Clark, M. Maglione, A. Laukkanen, I. E. Castelli, J. Carrasco, M. C. Cabanas, H. S. Stein, O. Ozcan, D. Elbert, K. Reuter, C. Scheurer, M. Demura, S. S. Han, T. Vegge, S. Nakamae, M. Fabrizio, and M. Kozdras, “Materials Acceleration Platforms (MAPs): Accelerating Materials Research and Development to Meet Urgent Societal Challenges,” *Advanced Materials*, vol. 36, no. 45, p. 2407791, Nov. 2024.
- [14] U. Nwabara, K. Yang, A. Talekar, V. Bernalles, J. González, S. Miller, and J. Wu, “High throughput computational and experimental methods for accelerated electrochemical materials discovery,” *J. Mater. Chem. A*, vol. 13, no. 32, pp. 26 041–26 066, 2025.
- [15] N. Pimenova and T. L. Starr, “Electrochemical Corrosion Investigation of 49-Cell Combinatorial Library of Titanium-Based Alloys Fabricated by DMD,” *J. Electrochem. Soc.*, vol. 155, no. 6, p. C303, 2008.

- [16] S. R. Taylor, “The investigation of corrosion phenomena with high throughput methods: A review,” *Corrosion Reviews*, vol. 29, no. 3-4, pp. 135–151, Oct. 2011.
- [17] P. White, G. Smith, T. Harvey, P. Corrigan, M. Glenn, D. Lau, S. Hardin, J. Mardel, T. Markley, T. Muster, N. Sherman, S. Garcia, J. Mol, and A. Hughes, “A new high-throughput method for corrosion testing,” *Corrosion Science*, vol. 58, pp. 327–331, May 2012.
- [18] P. Shi, B. Li, J. Huo, and L. Wen, “A Smart High-Throughput Experiment Platform for Materials Corrosion Study,” *Scientific Programming*, vol. 2016, pp. 1–9, 2016.
- [19] B. H. R. Gerroll, K. M. Kulesa, C. A. Ault, and L. A. Baker, “Legion: An Instrument for High-Throughput Electrochemistry,” *ACS Meas. Sci. Au*, vol. 3, no. 5, pp. 371–379, Oct. 2023.
- [20] H. Joress, B. DeCost, N. Hassan, T. M. Braun, J. M. Gorham, and J. Hatrick-Simpers, “Development of an automated millifluidic platform and data-analysis pipeline for rapid electrochemical corrosion measurements: A pH study on Zn-Ni,” *Electrochimica Acta*, vol. 428, p. 140866, Oct. 2022.
- [21] B. DeCost, H. Joress, S. Sarker, A. Mehta, and J. Hatrick-Simpers, “Towards Automated Design of Corrosion Resistant Alloy Coatings with an Autonomous Scanning Droplet Cell,” *JOM*, vol. 74, no. 8, pp. 2941–2950, Aug. 2022.
- [22] I. Oh, M. A. Pence, N. G. Lukhanin, O. Rodríguez, C. M. Schroeder, and J. Rodríguez-López, “The Electrolab: An open-source, modular platform for automated characterization of redox-active electrolytes,” *Device*, vol. 1, no. 5, p. 100103, Nov. 2023.
- [23] E. Rial-Rodríguez, J. D. Williams, D. Cantillo, T. Fuchß, A. Sommer, H.-M. Eggenweiler, C. O. Kappe, and G. Laudadio, “An Automated Electrochemical Flow Platform to Accelerate Library Synthesis and Reaction Optimization,” *Angew Chem Int Ed*, vol. 63, no. 51, p. e202412045, Dec. 2024.
- [24] K. J. Jenewein, K. Kan, D. Guevarra, R. J. R. Jones, Y. Lai, S. K. Suram, J. A. Haber, S. Cherevko, and J. M. Gregoire, “Automated monitoring of electrocatalyst corrosion as a function of electrochemical history and electrolyte formulation,” *Chem. Commun.*, vol. 60, no. 71, pp. 9554–9557, 2024.

- [25] H. Quinn, G. A. Robben, Z. Zheng, A. L. Gardner, J. G. Werner, and K. A. Brown, “PANDA: A self-driving lab for studying electrodeposited polymer films,” *Mater. Horiz.*, vol. 11, no. 21, pp. 5331–5340, 2024.
- [26] H. Sheng, J. Sun, O. Rodríguez, B. B. Hoar, W. Zhang, D. Xiang, T. Tang, A. Hazra, D. S. Min, A. G. Doyle, M. S. Sigman, C. Costentin, Q. Gu, J. Rodríguez-López, and C. Liu, “Autonomous closed-loop mechanistic investigation of molecular electrochemistry via automation,” *Nat Commun*, vol. 15, no. 1, p. 2781, Mar. 2024.
- [27] J. Abed, Y. Bai, D. Persaud, J. Kim, J. Witt, J. Hatrick-Simpers, and E. H. Sargent, “AMPERE: Automated modular platform for expedited and reproducible electrochemical testing,” *Digital Discovery*, vol. 3, no. 11, pp. 2265–2274, 2024.
- [28] K. Darvish, M. Skreta, Y. Zhao, N. Yoshikawa, S. Som, M. Bogdanovic, Y. Cao, H. Hao, H. Xu, A. Aspuru-Guzik, A. Garg, and F. Shkurti, “ORGANA: A robotic assistant for automated chemistry experimentation and characterization,” *Matter*, vol. 8, no. 2, p. 101897, Feb. 2025.
- [29] N. Fisker-Bødker, D. Persaud, Y. Bai, M. Kozdras, T. Vegge, J. Hatrick-Simpers, and J. H. Chang, “AMPERE-2: An open-hardware, robotic platform for automated electrodeposition and electrochemical validation,” *Digital Discovery*, vol. 4, no. 9, pp. 2491–2501, 2025.
- [30] M. Christensen, L. P. E. Yunker, P. Shiri, T. Zepel, P. L. Prieto, S. Grunert, F. Bork, and J. E. Hein, “Automation isn’t automatic,” *Chem. Sci.*, vol. 12, no. 47, pp. 15 473–15 490, 2021.
- [31] D. Adam, “The automated lab of tomorrow,” *Proc. Natl. Acad. Sci. U.S.A.*, vol. 121, no. 17, p. e2406320121, Apr. 2024.
- [32] “Standard Practice for Laboratory Immersion Corrosion Testing of Metals,” 1999.
- [33] G01 Committee, “Test Method for Conducting Cyclic Potentiodynamic Polarization Measurements for Localized Corrosion Susceptibility of Iron-, Nickel-, or Cobalt-Based Alloys.”
- [34] Carlos Mongay and Victor Cerda, “A Britton-Robinson Buffer of Known Ionic Strength,” *Ann. Chim*, vol. 64, no. 5, p. 5, 1974.

- [35] K. M. Kulesa, E. A. Hirtzel, V. T. Nguyen, D. P. Freitas, M. E. Edwards, X. Yan, and L. A. Baker, “Interfacing High-Throughput Electrosynthesis and Mass Spectrometric Analysis of Azines,” *Anal. Chem.*, vol. 96, no. 21, pp. 8249–8253, May 2024.
- [36] H. Zeng, Y. Yang, M. Zeng, and M. Li, “Effect of dissolved oxygen on electrochemical corrosion behavior of 2205 duplex stainless steel in hot concentrated seawater,” *Journal of Materials Science & Technology*, vol. 66, pp. 177–185, Mar. 2021.
- [37] P. C. Pistorius and G. T. Burstein, “Metastable pitting corrosion of stainless steel and the transition to stability,” *Phil. Trans. R. Soc. Lond. A*, vol. 341, no. 1662, pp. 531–559, Dec. 1992.
- [38] P. Delahay, M. Pourbaix, and P. Van Rysselberghe, “Potential-pH diagrams,” *J. Chem. Educ.*, vol. 27, no. 12, p. 683, Dec. 1950.
- [39] L. Bertolini, F. Bolzoni, M. Gastaldi, T. Pastore, P. Pedferri, and E. Redaelli, “Effects of cathodic prevention on the chloride threshold for steel corrosion in concrete,” *Electrochimica Acta*, vol. 54, no. 5, pp. 1452–1463, Feb. 2009.
- [40] P. Pedferri, “Cathodic protection and cathodic prevention,” *Construction and Building Materials*, vol. 10, no. 5, pp. 391–402, Jul. 1996.
- [41] Ja. M. Kolotyrkin, “Pitting Corrosion of Metals,” *Corrosion*, vol. 19, no. 8, pp. 261t–268t, Aug. 1963.
- [42] G. Flint, “Resistance of stainless steel to corrosion in naturally occurring waters,” 1980.
- [43] D. A. Jones, *Principles and Prevention of Corrosion*, 2nd ed. Upper Saddle River, NJ: Prentice Hall, 1996.

Data and Code Availability

The data that support this study, along with the analysis functions used to process the electrochemical measurements, are available in a public GitHub repository.

Acknowledgements

We acknowledge funding from Natural Sciences and Engineering Research Council of Canada, grant #RGPIN-2023-04843. The research was also, in part, made possible thanks to funding provided to the University of Toronto's Acceleration Consortium by the Canada First Research Excellence Fund (CFREF-2022-00042). Certain equipment, instruments, software, or materials are identified in this paper in order to specify the experimental procedure adequately. Such identification is not intended to imply recommendation or endorsement of any product or service by NIST, nor is it intended to imply that the materials or equipment identified are necessarily the best available for the purpose.

Author Contributions

Contributions are defined here after CRediT (the Contributor Roles Taxonomy). D.P: Conceptualization, Methodology, Software, Validation, Formal analysis, Investigation, Data Curation, Writing - Original Draft, Writing - Review & Editing, Visualization, Project administration. M.W: Methodology, Software, Validation, Writing - Original Draft, Writing - Review & Editing. M.X: Methodology, Software, Validation, Resources, Writing - Review & Editing. M.Z: Software. F.B: Resources. X.P: Supervision, V.A: Supervision. B.D: Supervision. A.D: Supervision. N.S: Supervision. G.B: Methodology, Resources, Writing - Original Draft, Funding acquisition. J.H.S: Conceptualization, Writing - Review & Editing, Supervision, Funding acquisition.

Competing Interests

The authors declare no competing interests.